Electrochemical Na-insertion/extraction properties of Sn−P anodes

Hiroyuki USUI[a,b], *Takuma SAKATA*[a,b], *Masahiro SHIMIZU*[a,b], *and Hiroki SAKAGUCHI*[a,b,*]

[a]Department of Chemistry and Biotechnology, Graduate School of Engineering, Tottori University, 4-101 Minami, Koyama-cho, Tottori 680-8552, Japan

[b]Center for Research on Green Sustainable Chemistry, Tottori University, 4-101 Minami, Koyama-cho, Tottori 680-8552, Japan

*Corresponding author. Tel./Fax: +81-857-31-5265; e-mail: sakaguch@chem.tottori-u.ac.jp

Abstract

Thick-film electrodes of tin phosphides, Sn_4P_3 and SnP_3, were prepared using a mechanical alloying method followed by a gas-deposition method, and were evaluated as Na-ion battery anodes in an organic electrolyte and ionic liquid electrolytes. The Sn_4P_3 electrode showed a better cycling performance in the organic electrolyte compared with the SnP_3 electrode and an Sn electrode. The performance of the Sn_4P_3 electrode was further improved by using ionic liquid electrolytes because of a uniformly formed surface layer and resulting uniform sodiation/desodiation reactions on the electrode.

Keywords: Tin phosphide; Na-ion battery anode; Mechanical alloying; Ionic liquid electrolyte

1. Introduction

Power generations based on renewable energy sources such as solar, wind, and geothermal are very important to realize a low-carbon society. Na-ion battery (NIB) has a disadvantage compared with Li-ion battery (LIB) in terms of the specific capacity of electrode and the energy density because of 2.4 times larger ionic volume of Na^+ than Li^+. On the other hand, sodium resources are available everywhere and much less expensive than lithium resources, which enables low-cost and large-scale production of NIB. Thus, NIB is a promising substitute for LIB in large-sized stationary batteries for the renewable energies. Komaba *et al.* have succeeded in bringing out an NIB anode of hard carbon a reversible capacity of 250−300 mA h g^{-1} by a reversible Na-insertion into its nanopores.[1] For a further high capacity, elemental phosphorous (P)[2] and tin (Sn)[3] are promising candidates of anode materials because these elements show high theoretical capacities (P, 2596 mA h g^{-1}; Sn, 847 mA h g^{-1}) based on alloying/dealloying reactions. Anodes consisting of elemental P or Sn, however, generally show deterioration of an active material layer and a resulting capacity decay by several ten cycles because these elements exhibit significant volume increase in their Na-storage ($Na_{15}Sn_4$, 525%; Na_3P, 490%).

Some researchers have developed Sn_4P_3 anodes.[4-6] It has been recently reported that Sn_4P_3 showed a synergistic Na-storage reaction where Sn and P atoms can react with Na to form $Na_{15}Sn_4$ and Na_3P, and that the resulting $Na_{15}Sn_4$ alloy acts as a conducting pathway to activate the reversible Na-storage reaction of nonconductive Na_3P particles while the well-dispersed Na_3P phase provides a shield matrix to prevent the aggregation of the $Na_{15}Sn_4$/Sn nanoparticles.

As new NIB anode materials, the authors have developed SnO,[7] SiO,[8] and TiO_2(rutile).[9] On the other hand, the authors have demonstrated a utility of an ionic liquid electrolyte for a high-capacity silicon anode in LIB: the electrolyte offered a better cycling performance of the anode by more homogeneous surface layer generated by its cathodic decomposition compared with that of a conventional organic electrolyte.[10-12] In this study, we investigated Na-insertion/extraction properties of Sn_4P_3 and SnP_3

electrodes in the organic electrolyte, and tried to improve the performance by applying the ionic liquid electrolyte.

2. Experimental

Active material powders of Sn_4P_3 and SnP_3 were prepared by a mechanical alloying (MA) method using commercially available tin (Kojundo Chemical Lab. Co., Ltd. 325 mesh, 99.99%) and amorphous red phosphorous (Wako Pure Chemical Industries, Ltd. 98.0%) with weight ratios of 4:3 and 1:3, respectively. The mixtures of tin and phosphorous powders were put in a stainless steel vessel together with balls so that the weight ratio of the active material and the balls was 1:30. The vessel used was sealed to keep an atmosphere of dry argon gas. The MA was carried out by using a high-energy planetary ball mill (P-6, Fritsch) for 10 hours with a rotation speed of 380 rpm at room temperature to obtain Sn_4P_3 and SnP_3 powders. In this study, we could not synthesized other binary alloys such as SnP and Sn_3P. For comparison, a black phosphorus powder was also prepared via MA from the red phosphorus powder. A commercial Sn powder (Kojundo Chemical Lab. Co., Ltd. 325 mesh, 99.99%) alone was also used as active material. The crystal structure of the powders was confirmed by using X-ray diffraction (XRD, Ultima IV, Rigaku).

Thick-film electrodes were prepared by a gas-deposition (GD) method.[13] This method is very beneficial for evaluating an original electrochemical property of an active material because it does not require any binder and conductive additive to prepare electrodes. GD was performed by using a nozzle with 0.5 mm in diameter, an Ar carrier gas with a purity of 99.99% under a differential pressure of 7.0×10^5 Pa, and a current collector of Cu foil substrate with 20 μm in thickness.

Na-insertion/extraction properties of the electrodes were evaluated in 2032-type coin cells. We assembled the electrodes as a working electrode, Na metal sheets (Rare Metallic, 99.8%) as counter electrode, and NaTFSA (sodium bis(trifluoromethanesulfonyl)amide, Kishida Chemical Co., Ltd.) dissolved in propylene carbonate (PC; $C_4H_6O_3$, Kishida Chemical Co., Ltd.) at a concentration of 1 M as

the electrolyte. Galvanostatic charge–discharge tests were carried out using an electrochemical measurement system (HJ-1001 SM8A, Hokuto Denko Co., Ltd.) at 303 K with potential ranges of 0.005–2.000 V vs. Na/Na^+. The current densities were set to be 50 mA g^{-1}. In addition, ionic liquid electrolytes were also studied for the electrodes. We used two kinds of ionic liquid electrolytes, 1 M NaTFSA-dissolved *N*-methyl-*N*-propylpyrrolidinium bis(fluorosulfonyl)amide (Py13-FSA) and 1-ethyl-3-methylimidazolium bis(fluorosulfonyl)amide (EMI-FSA).

The MA, the GD, and the cell assembly were performed throughout in a purge-type glove box (Miwa MFG, DBO-2.5LNKP-TS) filled with an Ar atmosphere in which an oxygen concentration and a dew point were below 1 ppm and –100°C, respectively.

3. Results and discussion

Figure 1 shows the galvanostatic charge (sodiation) and discharge (desodiation) potential profiles of the Sn_4P_3 and SnP_3 electrodes in the conventional organic electrolyte (NaTFSA/PC) at the first cycles. For comparison, the figure shows the results for the electrodes of black-P and Sn. The initial discharge capacity was increased with increasing the composition ratio of P in the active materials. The Sn_4P_3 and SnP_3 electrodes exhibited initial capacities larger than 250–300 mA h g^{-1}, typical capacities obtained for hard carbon-based electrodes.[1] Potential shoulders at 0.2–0.5 V and 0.5–1.2 V in the discharge profiles probably originate from desodiation reactions of Na–Sn and Na–P phases, respectively. It is suggested that the tin phosphides underwent a phase separation into Sn and P in the charge reaction at the first cycle.

To elucidate the mechanism, we performed *ex-situ* XRD measurement for the Sn_4P_3 electrode during the first charge−discharge reactions (Fig. 2). Sharp peaks at 21.6° and 31.5° were caused by an organic protective film covering the electrode surface. In the charge process, the diffraction peaks of Sn_4P_3 disappeared. New diffraction peaks, appeared at around 19.0° and 33.0°, can be possibly attributed to $Na_{15}Sn_4$ phase (Inorganic Crystal Structure Database, ICSD No.03-065-2166). At the fully discharged

state at 2.0 V, we did not observed Sn_4P_3, Sn, and P, indicating the amorphization of Sn and P. According to the reaction mechanism reported by Yang *et al.*,[4] we consider that the Sn_4P_3 electrode probably showed charge−discharge reactions described as following equations:

(Sodiation at the first cycle) $Sn_4P_3 + 24Na^+ + 24e^- \rightarrow Na_{15}Sn_4 + 3Na_3P$ (1)

(Sodiation/desodiation at the subsequent cycles) $Na_{15}Sn_4 \rightleftarrows 4Sn + 15Na^+ + 15e^-$ (2)

$Na_3P \rightleftarrows P + 3Na^+ + 3e^-$ (3)

Figure 3 represents cycling performances of the Sn_4P_3 and SnP_3 electrodes as compared with those of electrodes using Sn alone and P alone. The discharge capacity of the Sn electrode rapidly decreased by the initial five cycles. This poor cyclability originates from the volume expansion during sodiation, the aggregation during desodiation, and the resulting deterioration of active material layer.[5] In contrast, the Sn_4P_3 and SnP_3 electrodes showed an improved cyclability. In particular, the Sn_4P_3 electrode exhibited a better performance: the capacities over 400 mA h g^{-1} was maintained until the 25th cycle. The reason for the improved cyclability is probably the complementary effects of Na-storage reactions of Sn and P in the Sn−P alloys.[4-6] $Na_{15}Sn_4$ alloy acts as a conducting pathway to activate the reversible Na storage reaction of nonconductive Na_3P particles. In addition, the well-dispersed Na_3P phase provides a shielding matrix to prevent the aggregation of Sn. Nevertheless, a capacity decay was observed after the 26th cycle, which is similar to that of the P electrode. These results were presumably caused by large volumetric changes of P during sodiation and desodiation.

For a silicon anode for LIB having a high theoretical capacity and large volumetric changes during charge/discharge, we have revealed that some ionic liquid electrolytes are very effective to improve its anode performance.[10-12] In a conventional organic electrolyte, a thick surface layer with inhomogeneous thickness was formed on the electrode. This leads to intensive Li-insertion/extraction reactions on specific regions coated with thinner layer and an accelerated deterioration of Si active material layer.[12] On the other hand, the intensive reactions and the deterioration were effectively suppressed in an ionic liquid electrolyte because a uniform-thickness surface layer was formed due to its high electrochemical

stability.[12] Expecting similar improvement in the performance, we applied two kinds of ionic liquid electrolytes to the Sn_4P_3 electrode.

Figure 4 shows dependence of discharge capacities on cycle numbers for the Sn_4P_3 electrodes in ionic liquid electrolytes using Py13-FSA and EMI-FSA. The capacity fading was relatively suppressed by using EMI-FSA. In case of Py13-FSA, the cyclability was further improved: the capacity of 280 mA h g^{-1} was attained at the 50th cycle. As the authors expected, the ionic liquid electrolytes probably formed thin and uniform surface layers. This consideration is supported by higher initial Coulombic efficiencies of the ionic liquids (Py13-FSA: 78%, EMI-FSA: 75%) compared with the organic electrolyte (PC: 54%). With respect to EMI-FSA, it is suggested that the cathodic decomposition of EMI cation occurs by an initial attack on an acidic proton attached to the ring carbon between two nitrogen, which leads to a successive alkylation of the ring even after the second cycle and the resulting performance degradation. The superiority of Py13-based electrolyte to EMI-based electrolyte has been confirmed for Si-based LIB anodes.[11,14] In addition to this, Nohira and Hagiwara *et al.* have reported that Py13-FSA is useful for $NaCrO_2$ cathode.[15] These results indicate that Py13-FSA can improve the performance because it probably forms thin and uniform surface layer to allow uniform sodiation/desodiation reactions on the electrode.

4. Conclusion

We prepared the Sn_4P_3 and SnP_3 electrodes by using the MA method and the following GD method, and investigated their Na-insertion/extraction properties as NIB anodes. These electrodes showed larger initial reversible capacities in the conventional organic electrolyte than the capacity of 250–300 mA h g^{-1} obtained for hard carbon-based electrodes. The formation of $Na_{15}Sn_4$ phase was suggested for the sodiation state of the Sn_4P_3 electrode. The Sn_4P_3 and SnP_3 electrodes showed better cycling performances compared with the electrode of Sn alone. The improvements in the performances are probably attributed to complementary effects of $Na_{15}Sn_4$ and Na_3P formed in the electrodes on sodiation/desodiation

reactions of Sn and P: $Na_{15}Sn_4$ alloy acts as a conducting pathway to activate the reversible sodiation of nonconductive Na_3P particles, while the well-dispersed Na3P phase provides a shield matrix preventing Sn aggregation. The performance of the Sn_4P_3 electrode was further improved by using the ionic liquid electrolytes because of the uniformly formed surface layer and the resulting uniform sodiation/desodiation reactions on the electrode.

Acknowledgments

This work has been partially supported by Japan Society for the Promotion of Science (JSPS) KAKENHI, Grant-in-Aid for Scientific Research (B) (Grant Number 24350094) and Grant-in-Aid for JSPS Fellows (No. 2611485).

References

1. S. Komaba, W. Murata, T. Ishikawa, N. Yabuuchi, T. Ozeki, T. Nakayama, A. Ogata, K. Gotoh, and K. Fujiwara, *Adv. Funct. Mater.*, **21**, 3859 (2011).

2. N. Yabuuchi, Y. Matsuura, T. Ishikawa, S. Kuze, J.-Y. Son, Y.-T. Cui, H. Oji, and S. Komaba, *ChemElectroChem*, **1**, 580 (2014).

3. S. Komaba, Y. Matsuura, T. Ishikawa, N. Yabuuchi, W. Murata, and S. Kuze, *Electrochem. Commun.*, **21**, 65 (2012).

4. J. Qian, Y. Xiong, Y. Cao, X. Ai, and H. Yang, *Nano Lett.*, **14**, 1865 (2014).

5. Y. Kim, Y. Kim, A. Choi, S. Woo, D. Mok, N.-S. Choi, Y. S. Jung, J. H. Ryu, S. M. Oh, and K. T. Lee, *Adv. Mater.*, **26**, 4139 (2014).

6. J. Y. Jang, Y. Lee, Y. Kim, J. Lee, S.-M. Lee, K. T. Lee, and N.-S. Choi, *J. Mater. Chem. A*, **3**, 8332 (2015).

7. M. Shimizu, H. Usui, and H. Sakaguchi, *J. Power Sources*, **248**, 378 (2014).

8. M. Shimizu, H. Usui, K. Fujiwara, K. Yamane, and H. Sakaguchi, *J. Alloys Compd.*, **640**, 440 (2015).

9. H. Usui, S. Yoshioka, K. Wasada, M. Shimizu, and H. Sakaguchi, *ACS Appl. Mater. Interfaces*, **7**, 6567 (2015)

10. H. Usui, Y. Yamamoto, K. Yoshiyama, T. Itoh, and H. Sakaguchi, *J. Power Sources*, **196**, 3911 (2011).

11. H. Usui, T. Masuda, and H. Sakaguchi, *Chem. Lett.*, **41**, 521 (2012).

12. M. Shimizu, H. Usui, T. Suzumura, and H. Sakaguchi, *J. Phys. Chem. C*, **119**, 2975 (2015).

13. H. Sakaguchi, T. Toda, Y. Nagao, and T. Esaka, *Electrochem. Solid-State Lett.*, **10**, J146 (2007).

14. H. Usui, M. Shimizu, and H. Sakaguchi, *J. Power Sources*, **235**, 29 (2013).

15. C. Ding, T. Nohira, R. Hagiwara, K. Matsumoto, Y. Okamoto, A. Fukunaga, S. Sakai, K. Nitta, S. Inazawa, *J. Power Sources*, **269**, 124 (2014).

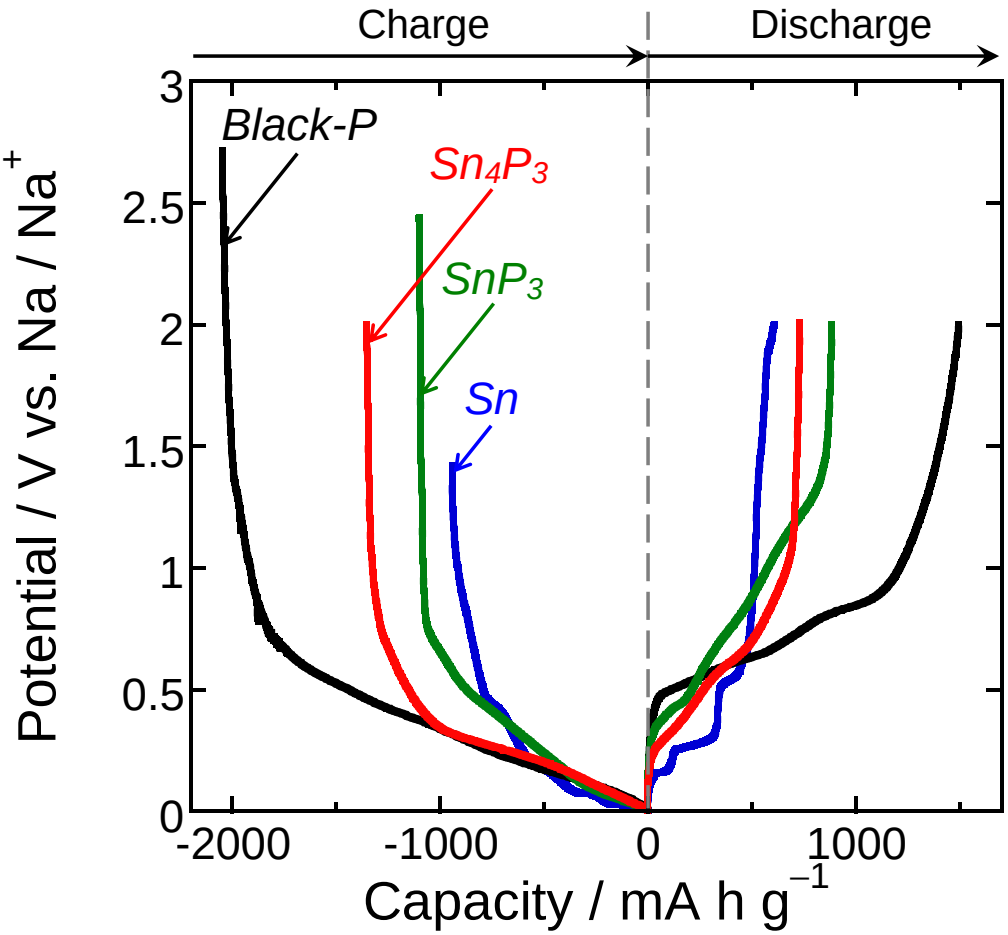

Figure 1. Galvanostatic charge (Na-insertion) and discharge (Na-extraction) profiles of Sn_4P_3 and SnP_3 electrodes at the first cycle under the current density of 50 mA g^{-1}.

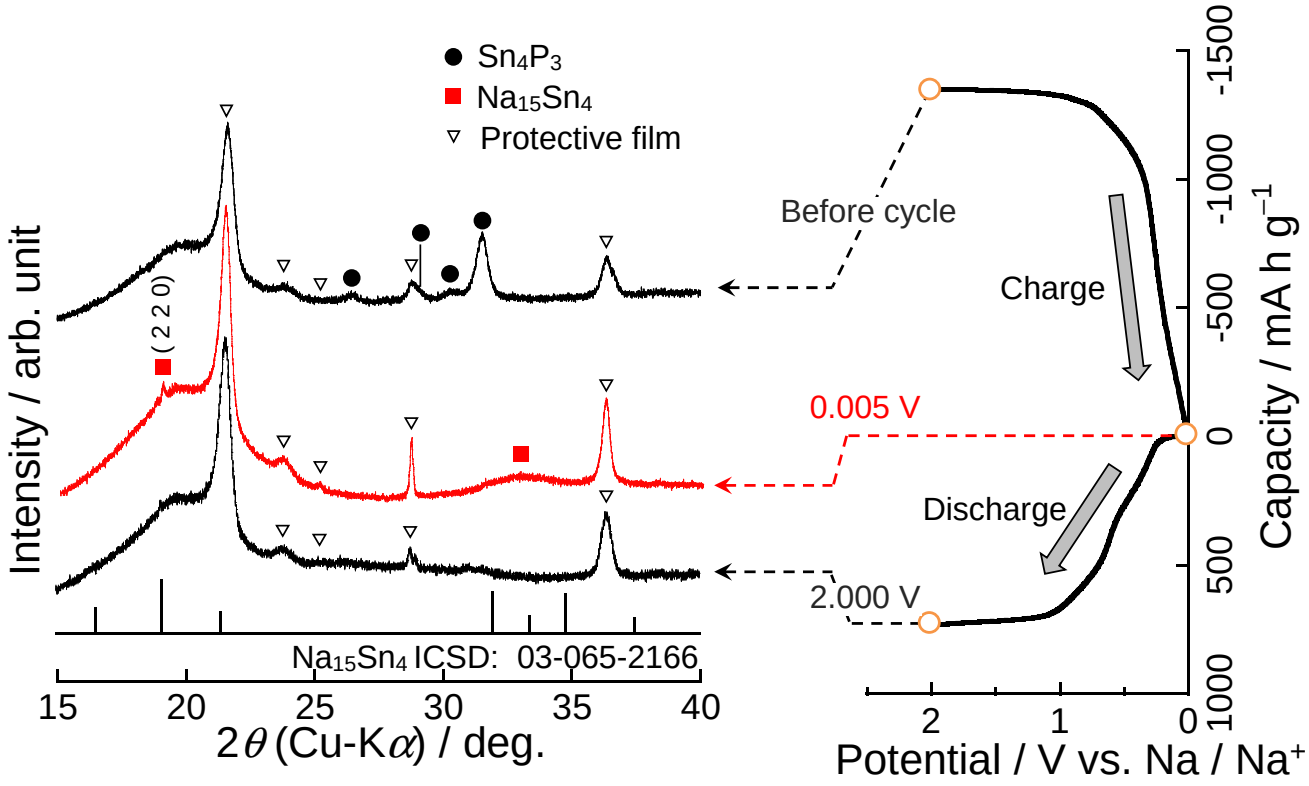

Figure 2. *Ex-situ* XRD patterns of the Sn_4P_3 electrode during the first cycle.

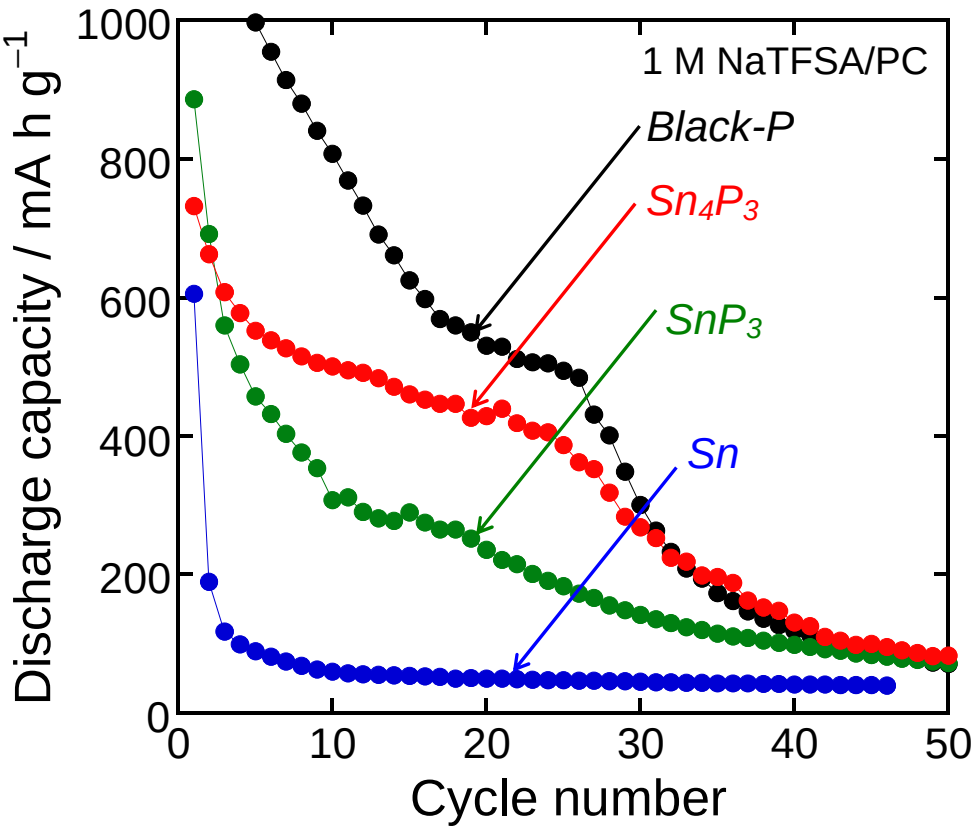

Figure 3. Cycling performances of the Sn_4P_3 and SnP_3 electrodes in conventional organic electrolyte (NaTFSA/PC). For comparison, the results of black-P and Sn electrodes were also shown in the figure.

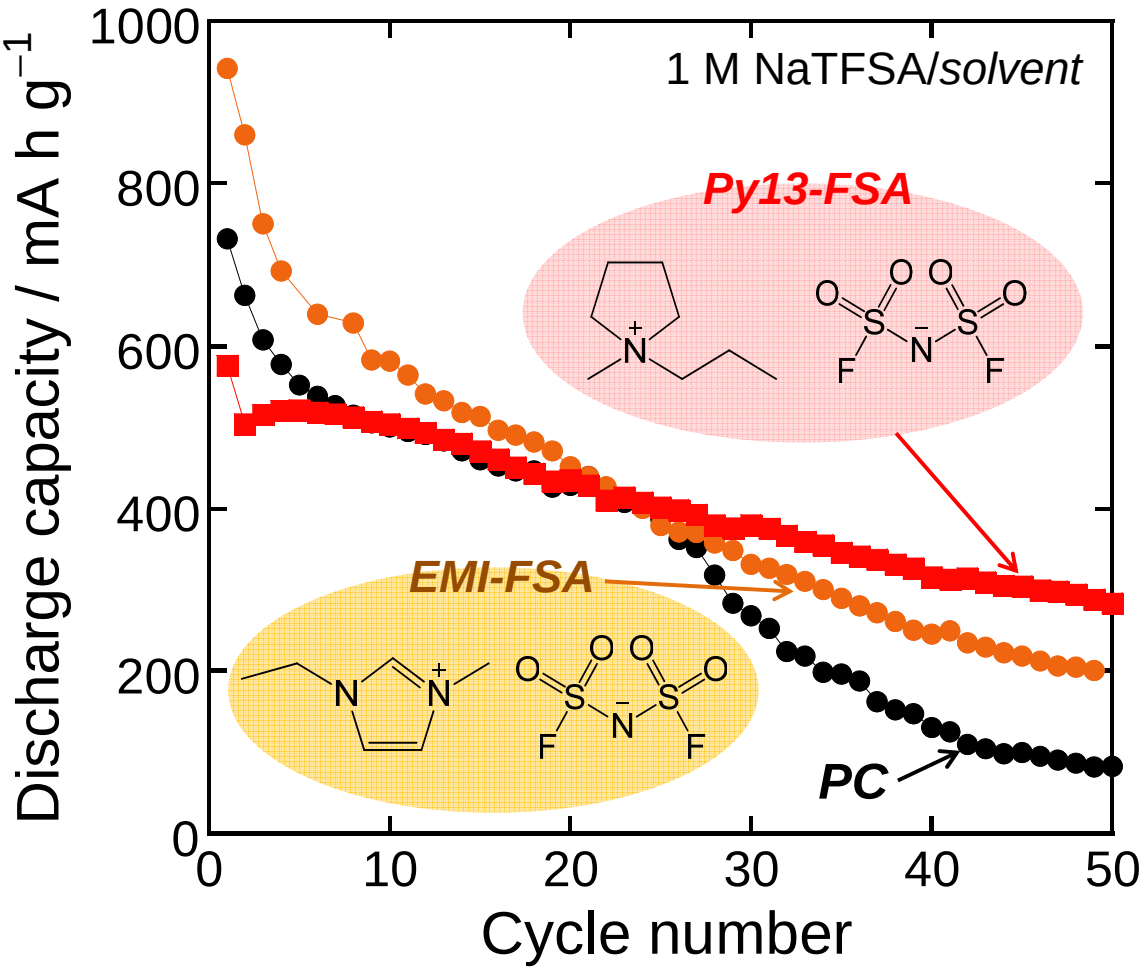

Figure 4. Dependence of discharge capacities on cycle numbers for the Sn_4P_3 electrodes in ionic liquid electrolytes (NaTFSA/Py13-FSA and NaTFSA/EMI-FSA).